*3. Manuscript
Click here to view linked References

The BOLD correlates of the visual P1 and N1 in single-trial analysis of simultaneous EEG-fMRI recording during a spatial detection task

Novitskiy N.[a], Ramautar J.R.[a,b], Vanderperren K.[c], De Vos M. [c], Vanrumste B.[c,d], Stiers P.[e], Van den Bergh B.[a,f], Lagae L.[b], Sunaert S.[g], Van Huffel S.[c], Wagemans J.[a]

[a]Katholieke Universiteit Leuven, Department of Psychology, Laboratory of Experimental Psychology, Leuven, Belgium

[b]Katholieke Universiteit Leuven, Department of Pediatric Neurology, Leuven, Belgium

[c]Katholieke Universiteit Leuven, Department of Electrical Engineering, ESAT-SCD, Leuven, Belgium

[d]Katholieke Hogeschool Kempen, Biosciences and Technology Department, Geel, Belgium

[e]Maastricht University, Faculty of Psychology and Neuroscience, Maastricht, The Netherlands

[f]Tilburg University, Department of Psychology, Tilburg, The Netherlands

[g]Katholieke Universiteit Leuven, Department of Radiology, Leuven, Belgium

Abstract:

The early stages of visual perception are characterized by both fast temporal dynamics and involvement of multiple brain areas. Combined EEG-fMRI promises to provide both time and space resolution to disentangle these processes of early visual perception. We used simultaneous EEG-fMRI recording during a simple spatial detection task with central and peripheral stimuli to investigate the interaction between the temporal dynamics and the brain distribution of visual-stimulus related activity between 80 and 200 ms after stimulus presentation. In the event-related fMRI activations were found in the vicinity of the primary visual areas at the locations mirroring the stimulus position in the visual field , as expected, and also in the contralateral extrastriatal areas at the junction between the temporal and occipital lobe. The ERPs consisted of P1 and N1 components with maximal amplitudes in the contralateral hemisphere and multiple sources according to sLORETA source modeling. We then used the difference between the voltage at the occipital electrodes of the two

hemispheres in the single-trials at P1 and N1 latencies as regressors in the fMRI analysis. This ERP-instructed fMRI analysis revealed partly overlapping activations for P1 and N1 in the temporal-occipital junction. Our data demonstrate the viability of recording early visual ERPs to peripheral stimuli inside the scanner. We suggest a novel method of using raw-EEG single trials for correlation with simultaneous fMRI.

Introduction:

Human perception is at the same time a fast and multi-component process. In the first 300-400 ms after stimulus onset our brain manages to fully analyze the stimulus and react to it. Different stages of that processing can be analyzed with event-related potentials (ERPs), a technique with millisecond time resolution. A typical ERP waveform is composed of components that correspond to different processing stages. The latencies of the peaks of the ERP components can then be used as a time mark for process timing in the brain.

Two ERP components P1 and N1 are ubiquitous in all visual studies (Odom et al., 2004), although under different names. In this paper the terminology most commonly used in cognitive neuroscience (Luck, 2005), will be used. This means that correspondingly at 100 ms and 180 ms after stimulus onset relevant changes in processing occur in the visual system. One quality that P1 and N1 share is retinotopy (e.g., Di Russo et al., 2002). In particular, both P1 and N1 responses are earlier and stronger over the hemisphere contralateral to the visual hemifield containing the stimulus. This similarity in retinotopic representation implies that the two components arise from the same source. If the activation of pyramidal neurons is the source of ERPs, it can be hypothetized that the surface positivity is created by a superficial source and thus by synaptic depolarizations at the level of the soma of pyramidal cells while the negativity is created by depolarizations at the level of apical dendrites(Nunez and Srinivasan, 2005). Thus, positivity and negativity may reflect the activity of the different

layers of the same cortical patch. Localization of the P1 and N1 sources with equivalent current dipole technique (ECD) gives contradictory results. Some authors locate the common source of the N1 and the P1 in the primary visual cortex, while others insist on an extrastriate origin of N1 or both components. The difference may also be due to the difference in stimulation, as most studies that reported primary sources used pattern reversal stimuli, while the ones with extrastriate sources used pattern onset stimuli (Di Russo et al., 2002; Di Russo et al., 2005). It is assumed that the N1 is more distributed across the brain than the P1, but it is not clear whether this is due to additional sources on top of shared ones or whether N1 activates a completely different set of sources. Some authors explicitly indicate the difficulty in localizing the N1 source as compared with the P1 source (Whittingstall et al., 2007).

However, experimental manipulations with P1 and N1 demonstrate a dissociation of those two ERP components. In an early invasive study, the GABA agonist bicuculline proved to increase the amplitude of the N1 but not the P1 components of the feline visual evoked responses (Zemon et al., 1980). The most pronounced differences between the P1 and N1 are reflected in their modulation by spatial attention (Fu et al., 2005; Luck et al., 1990; Noesselt et al., 2002). In the literature a discussion is going on about when the effect of attention appears in the visual ERPs. Some authors hold that the earliest cortical component C1 is free from attentional modulation (Martinez et al., 1999), while others explain the lack of the effect of attention on C1 due to imperfections of the earlier measurement techniques and the source localization models (Poghosyan and Ioannides, 2008). The effect of attention on P1 and N1 components is a generally accepted fact (Hillyard and Anllo-Vento, 1998). However, their behavior under attention is reported not to be identical. When the subject kept sustained attention on one visual hemifield, the N1 amplitude was increased only when the stimuli were presented unilaterally, while the P1 amplitude enhancement was noticed also with whole-

screen presentation (Luck et al., 1990). In another study, the N1 amplitude was increased under attention only when the subjects had to perform a discrimination task in the attended condition, while the P1 amplitude was larger for the attended location in both discrimination and simple detection tasks (Mangun and Hillyard, 1991). In both aforementioned studies the latencies of either the P1 or the N1 were not different in the attended and non-attended conditions. This suggests that the same neuronal populations are underlying both obligatory responses and that the attention effects are superimposed on it. Therefore, we may suppose that the dissociation exists also between obligatory P1 and N1 while it only becomes visible with an attention manipulation. In a series of studies Fu and colleagues (Fu et al., 2001; Fu et al., 2005) increased the attention of subjects to the stimuli by priming the location of the majority of the stimuli with a 4-dot cue. Interestingly, the N1 amplitude was smaller and its latency longer for primed (valid) as compared to non-primed stimuli. The P1 amplitude, on the other hand, was predictably larger in the valid than in the non-valid trials. Still, the latency of P1 was longer for valid trials. In another study, the proportion of the attended and non-attended parts of the visual field was manipulated. With an increased area of the attention span, the P1 amplitude increased while the N1 amplitude decreased (Luo et al., 2001). Other factors besides attention may help to dissociate N1 and P1. In an unattended condition, the amplitude of N1 was larger when the stimulus belonged to the same visual object as the cue, while the amplitude of P1 remained indifferent to that manipulation (Martinez et al., 2007). Predictability of the stimulus shortened the latency of N1, while no significant effects of predictability were found for P1 latency (Pollux and Guo, 2009).

The evidence mentioned above suggests that P1 and N1 may be generated by different neuronal populations. However, direct comparison of the P1 and N1 sources is a difficult task with the current methods. For instance, the inverse problem is complicated in case of ERP

components with a broad scalp voltage distribution, such as N1. Therefore, the spatial resolution of fMRI is required to solve this problem. The common neural sources of fMRI and EEG (Logothetis et al., 2001) support the assumption of common information in EEG and fMRI datasets. While important results have been obtained by a combination of fMRI and EEG data recorded in separate sessions (e.g., Di Russo et al., 2002, 2005), this approach has its limitations. Firstly, the physical environment, arousal state and attentional level of the experimental subject can be very different in EEG and fMRI recording sessions (Debener et al., 2005). Secondly, the separate sessions only allow combination of already averaged ERP and fMRI responses. A good example of this approach is the use of fMRI activations as seed for ERP dipole localizations (Bledowski et al., 2004). The obvious limitation is that instead of extracting common information,the information is forced from one method onto another. A more fruitful approach would be the combination of fMRI and ERP information on a single trial level. This approach requires simultaneous acquisition of fMRI and EEG. Interesting examples of such an approach are recent studies of the P3 component in an oddball paradigm (Benar et al., 2007),the error-related negativity (ERN) in a flanker task (Debener et al., 2005). Those and other studies (for reviews, see Eichele et al., 2009 and Calhoun et al., 2009), however, did not attempt to compare directly two ERP components with close latency. In the present study we simultaneously recorded EEG and fMRI during the performance of a simple detection task. The amplitude of P1 and N1 in individual epochs was used as a regressor in the fMRI analysis in order to define the sources of maximal variability in P1 and N1.

Methods:

Experimental subjects

10 subjects (7 males) participated in the study (age 21-33 years, median 25.5 years, one left-handed). They did not report any neurological diseases and had normal or corrected-to-normal

vision. During the presentation of the stimuli subjects were lying supine in the scanner on a cushion that ameliorated the pressure from the electrodes on the head. The head of the subject was fixed in the coil with soft cushions. Subjects were provided with earplugs to avoid harmful effect of fMRI acoustic noise.

Stimuli and presentation

The stimulation paradigm was generated and presented with the Presentation software (Neurobehavioral Systems, Albany, CA, USA). Quadrant segments of a circular checkerboard were projected from the technical room of the scanner to the plastic screen (17x25 cm) positioned at the upper internal surface of the scanner bore. The subject saw the screen reflection in the mirror positioned at the top of the head coil at the distance of 29 cm from the screen. The distance between the eyes and the screen was 6 cm. The segments (3.4x3.3 cm) were 6° (3.4x3.3 cm) in size and their centers were positioned at 8°(5 cm) distance from the fixation point. They were presented equiprobably with randomized stimulus-onset asynchronies (SOAs) to each of 4 quadrants: upper left (UL), upper right (UR), down-left (DL), and down-right (DR) (**Fig. 1A**). The subject was instructed to fixate at the fixation cross and to press a button whenever she detected a checkerboard. In addition, a full checkerboard with about 5° radius was presented centrally with the same probability as each of the segment positions. The stimuli were presented in 4 four blocks of 100 stimuli each. The SOA varied randomly from 1 to 2.5 s in 100 ms steps. Empty events were introduced in 38% of the cases to provide a baseline for the fMRI event-related analysis. The presence of an empty event added variability to the perceived SOA (**Fig. 1B**). The instructions, the random order of the segment positions, the form of the segments, and the introduction of a central stimulus motivated the subject to keep central fixation. In the same session and intermingled with the

present task (but in different blocks), the subject performed another task which is not considered in this paper and which will be reported elsewhere.

In addition to the recordings inside the scanner, a subset of the subjects performed the same tasks outside the scanner to provide a clean EEG control. In that session the subject was watching the stimuli on a monitor of a computer from a sitting position and responded with a mouse click. We do not report the outside data in this paper. The comparison of inside (but without gradients) and outside data of the same subjects has been reported elsewhere (Assecondi et al., 2009).

Simultaneous EEG and fMRI recording

EEG was recorded with the Brain Amp+ system hardware and the Brain Vision Recorder software (BrainProducts,Munich, Germany). EEG was recorded at 5 kHz digitization rate with a 64-MRI compatible electrode cap from the scalp, which was fed via short cables to the amplifiers inside the scanner room. FCz was used as reference electrode and the inion position (Iz electrode) was used as ground electrode. Two channels of the electrode cap were used to record monopolar elecrooculogram (EOG) and electrocardiogram (ECG); the corresponding electrodes were attached under left eye and left shoulder blade of the subject. The impedance between electrode and scalp was kept below 10 kΩ. The MRI compatible amplifiers were placed at the edge of the scanner tube and the wires that connected the cap with the amplifier were fixed in their position with sand bags to avoid vibrations. The digital output from the amplifiers was fed into the laptop positioned outside the scanner via optical cables.

fMRI data were recorded with a Philips 3T Intera whole-body scanner. 160 echo-planar images (EPI) composed of 28 slices of 3x3x4.5 mm voxel size and 4.8 mm slice thickness were recorded with ascending slice order with 1.95 s repetition time (TR) during each experimental block.Full brain anatomical image was obtained with the magnetization

prepared rapid gradient echo **(**MPRAGE) imaging sequence (230 coronal slices, time to echo [TE]=4,6 ms, TR=9.7).

EEG preprocessing and analysis

EEG data were cleaned from gradient artifacts by template subtraction (Allen et al., 2000) with Brain Vision Analyzer software (BrainProducts, Munich, Germany). The data were then down-sampled to 250 Hz, low-pass filtered at 30 Hz and imported into MATLAB(The Mathworks Inc. Natick, Massachusetts, USA). Further analysis was done with the EEGLAB toolbox (Delorme and Makeig, 2004). The ballistocardiogram (BCG) artifact was removed with template subtraction based on the optimal basis set (OBS) method from the EEGLAB FMRIB tool (Niazy et al., 2005). The residual BCG artifact was removed with independent component analysis (ICA). More specifically, components that explained more than 10% of the variance in the ECG channel were removed. The combination of OBS and ICA has been previously shown to yield the best results in BCG removal (Debener et al., 2007), as long as precautions are taken not to remove too much of the activity (Vanderperren et al., submitted). The blink-related EEG activity was also removed with ICA. Blinks were detected on the EOG channel as a transient deflection in amplitude and the blink-related independent component was defined as the one that explained more than 10% of the variance at the EOG electrode in the blink-locked epochs (Mennes et al., in revision). The data were segmented from 100 ms before until 400 ms after around stimulus onset, artifact-rejected at 100 μV (rejection rate 22±5 %), baseline corrected (-100 – 0 ms) and re-referenced to the average of TP9 and TP10 (the closest electrodes to the mastoids in the present electrode setup). ERPs were averaged separately for responses to the stimuli in each of four quadrants and the central stimulus. In addition, the responses to all peripheral stimuli were pooled together to get a so-called contra-ipsilateral voltage map. To that end, first, the responses to the upper and lower visual fields

were averaged together and subsequently the responses to the right visual field were flipped around the central line and averaged together with the responses to the left visual field. P1 was measured as a positive deflection at the occipital electrodes in the 50-150 ms time window and N1 as a negative deflection in the 150-250 ms window. A set of 5 occipito-temporal electrodes in each of the left (O1, P7, PO3, P5, PO7) and right (O2, P8, PO4, P6, PO8) hemispheres was chosen to measure the amplitudes of the ERP, as P1 and N1 were best pronounced at those electrodes.

We performed a standardized low resolution brain electromagnetic tomography technique (sLORETA) for source localization at the peak latencies of P1 (108 ms) and N1 (180 ms) at the grand-average waveforms for each of the peripheral stimulus conditions (Pascual-Marqui, 2002).

fMRI preprocessing and analysis

fMRI analysis was performed with statistical parametric mapping software (SPM5, Wellcome Department of Cognitive Neurology, London, UK). The EPI time-series were slice-time corrected, realigned, co-registered with anatomical images, normalized and smoothed with an 8-mm FWHM Gaussian kernel using SPM5.

First-order statistics (fixed effect analyses) were calculated on the basis of convolution of a stick function at the stimulus timing with a canonical HRF function, separately for 5 stimulus locations. No derivativees were used in the analysis. The movement parameters obtained during the realignment were inserted in the model as covariates of no interest. As a result, the design consisted of 5+6=11 variables per experimental block per subject. In the analysis of second-order statistics (random-effect analysis), the contrasts of the 5 stimuli types and the baseline for each individual subject were used. We report the result of the contrast between

each peripheral stimulus type and all other peripheral stimuli as well as the contrast of the right- and left visual field responses against the baseline.

In addition, both first- and second-order statistics were computed to compare the trials where the stimulus was presented at the same location as in the previous trial with the ones where the location was different between two consecutive trials to control for possible effects of apparent motion (see Results and Discussion).

Brain structures were identified with a Munster T2T converter (http://wwwneuro03.uni-muenster.de/ger/t2tconv/conv3d.html) by the MNI coordinates of the cluster.

Combined EEG and fMRI analysis

For a combined analysis the cleaned, segmented, baseline-corrected and re-referenced EEG data were used. The averaged amplitudes in the individually measured time windows of P1 and N1 were measured at 5 occipital electrodes in each hemisphere in every epoch. Then the averaged amplitudes over the right hemisphere electrodes were subtracted from the averaged amplitudes in the left hemisphere. All difference values beyond 3 standard deviations from zero were substituted with the mean of the data within 3 standard deviations. This procedure has been repeated twice: for the raw amplitude single-electrode values and for the pooled difference values. The number of substituted trials at single electrodes was 6±0.3 for the P1 and 5±0.3 for the N1. The number of substituted trials in the pooled differences was 3±0.6 for the P1 and 3±0.5 for the N1. We checked if the ERP regressor predicted the side of the stimulating visual field in each individual subject significantly higher than chance level.

The resulting vector of the amplitude differences was split according to the polarity of the amplitude difference (positive for larger amplitude in the left hemisphere) (**Fig. 2**). The negative numbers were substituted with their absolute values. This resulted in 2 vectors per

subject per block per ERP component. These vectors were convolved with the canonical hemodynamic response function (HRF) to create regressors for the fMRI analysis. The movement parameters were used as covariates of no interest just as in the standard fMRI analysis. Only first-order statistics (fixed-effect analysis) were performed at individual and group level, since the low signal-to-noise ratio did not allow random effects analysis. This naturally limits our conclusions to this specific group of subjects making the population effects subject to speculation. The threshold was defined as $p<0.05$ family-wise error (FWE) corrected. Brain structures were again identified with Munster T2T converter (http://wwwneuro03.uni-muenster.de/ger/t2tconv/conv3d.html) by the MNI coordinates of the cluster.

The activation cluster from the posterior brain have been used as regions of interest (ROIs). ROI analysis has been performed with MarsBaR SPM toolbox (Brett et al., 2002), http://marsbar.sourceforge.net/. The contrast in 4 ROIs (for P1 in the left hemisphere, P1 in the left hemisphere, N1 in the left hemisphere and N1 in the right hemisphere) was measured for each of 2 contrasts (right and left hemisphere) of 2 designs (P1 and N1 regression). The resulting contrasts were compared within each ROI between the hemispheres for each ERP component and between components within one hemisphere with a one-tailed t-test.

Results

EEG

Upper-left, upper-right, down-left, down-right and central stimuli elicited ERPs with a characteristic P1–N1 pattern (**Fig. 3**). One can distinguish contra- and, at a somewhat later latency, ipsilateral P1 and N1. In this study we concentrated on the contralateral components. Contralateral P1 had a latency of 108±6.8 ms and contralateral N1 had a latency of 189±3.3 ms.

The amplitude of the P1 and the N1 was measured as the average of a 3-sample (8 ms) window around the individual subject's latency for t he corresponding peak. The ERPs from the peripheral stimuli were pooled first, over upper and lower locations and then, after flipping across the midline, over right and left locations. The sign of amplitude was reversed in case of N1 to keep the same direction of change for the two components.

To compare the P1 and the N1 amplitudes for right and left visual fields, we ran a 4-way repeated measures ANOVA with factors condition (left visual field, right visual field and central), component (P1 and N1), hemisphere (right or left) and electrode (5 electrodes of the set). There were no significant main effects in that analysis. The significant interactions were: Condition X Hemisphere ($F(2,18)=30.1$, $p<0.001$), Condition X Electrode ($F(8,72)=3.9$, $p<0.05$), Condition X Component X Hemisphere ($F(2,18)=29.8$, $p<0.001$), and Condition X Hemisphere X Electrode ($F(8,72)=4.3$, $p<0.05$). Post-hoc comparison (t-test with Bonferroni correction) within the Condition X Component X Hemisphere interaction showed that the N1 amplitude to the stimulus in both left and right visual field and the P1 amplitude to the stimulus in the right visual field were larger in the contralateral than in the ipsilateral hemisphere (**Table 1**).

To compare the P1 and N1 amplitudes for upper and lower visual fields we ran a 4-way ANOVA with factors condition (upper or lower visual field), component (P1 and N1), laterality (contra- or ipsilateral) and electrode (5 electrodes of the set). The ERP amplitude was larger in the contra- than in the ipsilateral hemisphere ($F(1,9)=36.1$, $p<0.001$) and for the stimuli in the lower than in the upper visual field ($F(1,9)=19.1$, $p<0.01$). The latter result corroborates earlier magnetoencephalographic findings of stronger responses to lower than upper visual field at early latency (Portin et al., 1999). The following interactions were also significant: Condition X Component ($F(1,9)=20.4$, $p<0.01$), Component X Laterality

($F(1,9)=42.9$, $p<0.001$), Condition X Electrode ($F(4,36)=5.5$, $p<0.01$), Laterality X Electrode ($F(4,36)=7.3$, $p<0.01$), Condition X Component X Laterality ($F(1,9)=9.3$, $p<0.05$), and Condition X Component X Electrode ($F(4,36)=5.0$, $p<0.05$).

sLORETA results are presented in **Fig. 4.** The activations were present in occipital as well as frontal, temporal and parietal areas of the brain. Both the P1 and N1 for both left visual field (LVF) and right visual field (RVF) stimuli produced stronger contra- than ipsilateral activations in the lateral occipital cortex in the vicinity of middle occipital gyrus (MOG).

Event-related fMRI

Event-related fMRI results are presented in **Fig. 5** and **6**. The shown activations are significant in the random-effects group analysis with false discovery rate (FDR) corrected $p<0.05$, except for upper left condition where the threshold was $p<0.056$ (**Fig. 5**). The upper left stimulation produced activation in the right lingual gyrus and right cerebellum. The upper right stimulus produced activation in the left lingual gyrus and left cuneus. The down left stimuli activated the right cuneus and the down-right stimuli activated the left middle occipital gyrus (MOG) (**Table 3**).

The comparison of the right and left visual field activations against a baseline produced stronger activations than the previously described contrast of each of the stimuli against the rest of the stimuli. Therefore, to detect the former we used a more stringent threshold, namely family-wise corrected (FWE) $p<0.05$ (**Fig. 6**). Left visual field stimuli activated the right inferior temporal gyrus, right fusiform gyrus, right cuneus, left medial frontal gyrus, right precentral gyrus and right cuneus. Right visual field activated the left middle occipital gyrus, left fusiform gyrus, left medial frontal gyrus and left cerebellum (**Table 3**).

The contrast between the trials with the same and different preceding stimulus in the random-effects group analysis revealed no significant activation at false discovery rate corrected $p<0.05$.

EEG-directed fMRI

The predictive power of ERP regressors is summated in **Table 2.** In 3 subjects out of 10 the P1 regressor predicted the side of the stimulus significantly higher than chance. In 9 subjects out of 10, the prediction of the stimulus side by the N1 regressor was significantly higher than chance.

The fixed-effect analysis of trials with left-lateralized P1 revealed activations in the left middle occipital gyrus and right middle temporal gyrus. Right-lateralized P1 activated the right middle temporal gyrus, left precentral gyrus, left medial frontal gyrus and superior frontal gyrus (**Fig. 7, Table 4**).

The fixed-effect analysis of trials with left-lateralized N1 showed activations in the left middle occipital gyrus, left medial frontal gyrus, left precentral gyrus and right middle temporal gyrus. Right-lateralized N1 activated the right middle occipital gyrus and left precentral gyrus (**Fig. 7, Table 5).**

There was a tendency of the responses in the left-hemisphere ROIs to be higher for left hemisphere contrast and for N1 responses in the left hemisphere ROIs to be higher than P1 responses. However, only one comparison was significant: N1 contrast for the left hemisphere was higher than the N1 contrast for right hemisphere in the P1 left-hemisphere ROI.

Discussion:

In this study we suggested a method of integration of the simultaneously recorded EEG and fMRI data that make use of paradigm-induced differences between single trials of ERP. We

also demonstrated that it is possible to record ERPs to peripheral visual stimuli inside the scanner.

In a separate analysis of fMRI and EEG we found the expected results, despite the fact that the EEG data inside the scanner is noisier than the data outside. Still, the differences between ipsi- and contralateral responses were present for both the P1 and N1 components of the ERPs (**Fig. 3,4**) and the retinotopy was present in the fMRI data around both calcarine sulci (**Fig. 5**). These results strengthen our conviction that the experimental design, data recording and preprocessing were relevant and accurate. Note that the minimal SOA used (1 s) was shorter than the one normally recommended for event-related fMRI studies while it was quite long for sensory evoked potential studies.

In addition to the brain areas in vicinity of calcarine sulcus, we found activations in the lateral occipital cortex. Their MNI coordinates were close to those of area hMT+ (hV5). Usually, this area is activated when the stimuli are moving (Sunaert et al., 1999). One may suspect that the relatively fast presentation of the same stimulus in different locations may have created an illusion of apparent movement in the subjects. However, the direct comparison between the trials where the location of the stimulus was different in comparison with the previous stimulus and the ones where it was the same did not reveal any significant differences; the activation of MT was present in both conditions, so we have to look for other sources of MT activation. There are indeed data in the literature where MT was activated by the shape-discriminability manipulation of stationary stimuli (Kourtzi et al., 2002).

We extracted the precise time information of the ERP in the form of trial variation of the amplitude of the ERP components, P1 and N1. Since the main expected modulation is earlier and/or stronger at the contralateral side to the stimulus presentation, we used as a measure the difference between the left and right occipito-parietal electrodes in individual-trial amplitude

at the latency of the averaged contralateral component ERP peak. The assumption was that, on the one hand, both P1 and N1 would be captured by this measure, and, on the other hand, the subtle differences in the subtracted amplitude variation between two components will be enough to extract the areas in the brain that are more correlated to the variation in one and not the other of the two ERP components. The locations of fMRI activations to P1 and N1 regressors in the lateral occipital cortex (**Fig. 7**) were close to the results of standard fMRI analysis on one hand (**Fig.6**) and to the sLORETA resuts on the other hand (**Fig. 4**). That suggest the correctness of the first assumption. The locations of P1- and N1activations were only partly overlapping (**Fig.7**). That points to the correctness of the second assumption.

We conclude, firstly, that it is possible to obtain reliable event-related potentials inside the scanner with predictable paradigm-induced modulation for early visual components P1 and N1. Secondly, the individual trial variability of experiment-induced modulation can be used as a regressor in fMRI analysis to obtain insights into the spatio-temporal dynamics of early visual processing.

Acknowledgements

This research is supported by the Research Council KUL: IDO 05/010 EEG-fMRI and GOA-MANET, the Belgian Federal Science Policy Office IUAP P6/04 (DYSCO) and the EU project Neuromath (COST-BM0601). Katrien Vanderperren and Maarten De Vos are supported by a PhD grant from the Flemish Government (IWT). Nikolay Novitskiy is supported by a post-doctoral scholarship of Research Foundation – Flanders (FWO). Johan Wagemans is supported by a Methusalem grant by the Flemish Government (METH/08/02).

Literature:

Allen, P. J., Josephs, O., Turner, R., 2000. A method for removing imaging artifact from continuous EEG recorded during functional MRI. Neuroimage 12, 230-239.

Assecondi, S., Vanderperren, K., Novitskiy, N., Ramautar, J., Fias, W., Stiers, P., Sunaert, S., Staelens, S., Van Huffel, S., Lemahieu, I., 2009. Effect of the static magnetic field of the MR-scanner on ERPs: evaluation of visual, cognitive and motor potentials. Clinical Neurophysiology submitted.

Benar, C. G., Schon, D., Grimault, S., Nazarian, B., Burle, B., Roth, M., Badier, J. M., Marquis, P., Liegeois-Chauvel, C., Anton, J. L., 2007. Single-trial analysis of oddball event-related potentials in simultaneous EEG-fMRI. Hum Brain Mapp 28, 602-613.

Bledowski, C., Prvulovic, D., Hoechstetter, K., Scherg, M., Wibral, M., Goebel, R., Linden, D. E., 2004. Localizing P300 generators in visual target and distractor processing: a combined event-related potential and functional magnetic resonance imaging study. J Neurosci 24, 9353-9360.

Brett, M., Anton, J. L., Valabregne, R., Poline, J. B., 2002. Region of interest analysis using an SPM toolbox,8th International Conferance on Functional Mapping of the Human Brain, Sendai, Japan, p. abstract 497.

Calhoun, V. D., Liu, J., Adali, T., 2009. A review of group ICA for fMRI data and ICA for joint inference of imaging, genetic, and ERP data. Neuroimage 45, S163-172.

Debener, S., Strobel, A., Sorger, B., Peters, J., Kranczioch, C., Engel, A. K., Goebel, R., 2007. Improved quality of auditory event-related potentials recorded simultaneously with 3-T fMRI: removal of the ballistocardiogram artefact. Neuroimage 34, 587-597.

Debener, S., Ullsperger, M., Siegel, M., Fiehler, K., von Cramon, D. Y., Engel, A. K., 2005. Trial-by-trial coupling of concurrent electroencephalogram and functional magnetic resonance imaging identifies the dynamics of performance monitoring. J Neurosci 25, 11730-11737.

Delorme, A., Makeig, S., 2004. EEGLAB: an open source toolbox for analysis of single-trial EEG dynamics including independent component analysis. J Neurosci Methods 134, 9-21.

Di Russo, F., Martinez, A., Sereno, M. I., Pitzalis, S., Hillyard, S. A., 2002. Cortical sources of the early components of the visual evoked potential. Hum Brain Mapp 15, 95-111.

Di Russo, F., Pitzalis, S., Spitoni, G., Aprile, T., Patria, F., Spinelli, D., Hillyard, S. A., 2005. Identification of the neural sources of the pattern-reversal VEP. Neuroimage 24, 874-886.

Eichele, T., Calhoun, V. D., Debener, S., 2009. Mining EEG-fMRI using independent component analysis. Int J Psychophysiol 15, in press.

Fu, S., Fan, S., Chen, L., Zhuo, Y., 2001. The attentional effects of peripheral cueing as revealed by two event-related potential studies. Clin Neurophysiol 112, 172-185.

Fu, S., Greenwood, P. M., Parasuraman, R., 2005. Brain mechanisms of involuntary visuospatial attention: an event-related potential study. Hum Brain Mapp 25, 378-390.

Hillyard, S. A., Anllo-Vento, L., 1998. Event-related brain potentials in the study of visual selective attention. Proc Natl Acad Sci U S A 95, 781-787.

Kourtzi, Z., Bulthoff, H. H., Erb, M., Grodd, W., 2002. Object-selective responses in the human motion area MT/MST. Nat Neurosci 5, 17-18.

Logothetis, N. K., Pauls, J., Augath, M., Trinath, T., Oeltermann, A., 2001. Neurophysiological investigation of the basis of the fMRI signal. Nature 412, 150-157.

Luck, S. J., 2005. An introduction to the event-related potential technique The MIT Press, Cambridge, MA.

Luck, S. J., Heinze, H. J., Mangun, G. R., Hillyard, S. A., 1990. Visual event-related potentials index focused attention within bilateral stimulus arrays. II. Functional dissociation of P1 and N1 components. Electroencephalogr Clin Neurophysiol 75, 528-542.

Luo, Y. J., Greenwood, P. M., Parasuraman, R., 2001. Dynamics of the spatial scale of visual attention revealed by brain event-related potentials. Brain Res Cogn Brain Res 12, 371-381.

Mangun, G. R., Hillyard, S. A., 1991. Modulations of sensory-evoked brain potentials indicate changes in perceptual processing during visual-spatial priming. J Exp Psychol Hum Percept Perform 17, 1057-1074.

Martinez, A., Anllo-Vento, L., Sereno, M. I., Frank, L. R., Buxton, R. B., Dubowitz, D. J., Wong, E. C., Hinrichs, H., Heinze, H. J., Hillyard, S. A., 1999. Involvement of striate and extrastriate visual cortical areas in spatial attention. Nat Neurosci 2, 364-369.

Martinez, A., Ramanathan, D. S., Foxe, J. J., Javitt, D. C., Hillyard, S. A., 2007. The role of spatial attention in the selection of real and illusory objects. J Neurosci 27, 7963-7973.

Niazy, R. K., Beckmann, C. F., Iannetti, G. D., Brady, J. M., Smith, S. M., 2005. Removal of FMRI environment artifacts from EEG data using optimal basis sets. Neuroimage 28, 720-737.

Noesselt, T., Hillyard, S. A., Woldorff, M. G., Schoenfeld, A., Hagner, T., Jancke, L., Tempelmann, C., Hinrichs, H., Heinze, H. J., 2002. Delayed striate cortical activation during spatial attention. Neuron 35, 575-587.

Nunez, P. L., Srinivasan, R., 2005. Electric Fields of the Brain: The Neurophysics of EEG. Oxford University Press, USA.

Odom, J. V., Bach, M., Barber, C., Brigell, M., Marmor, M. F., Tormene, A. P., Holder, G. E., Vaegan, 2004. Visual evoked potentials standard (2004). Doc Ophthalmol 108, 115-123.

Pascual-Marqui, R. D., 2002. Standardized low-resolution brain electromagnetic tomography (sLORETA): technical details. Methods Find Exp Clin Pharmacol 24 Suppl D, 5-12.

Poghosyan, V., Ioannides, A. A., 2008. Attention modulates earliest responses in the primary auditory and visual cortices. Neuron 58, 802-813.

Pollux, P. M., Guo, K., 2009. Event-related potential correlates of spatiotemporal regularities in vision. Neuroreport 20, 525-530.

Portin, K., Vanni, S., Virsu, V., Hari, R., 1999. Stronger occipital cortical activation to lower than upper visual field stimuli. Neuromagnetic recordings. Exp Brain Res 124, 287-294.

Sunaert, S., Van Hecke, P., Marchal, G., Orban, G. A., 1999. Motion-responsive regions of the human brain. Exp Brain Res 127, 355-370.

Whittingstall, K., Stroink, G., Schmidt, M., 2007. Evaluating the spatial relationship of event-related potential and functional MRI sources in the primary visual cortex. Hum Brain Mapp 28, 134-142.

Zemon, V., Kaplan, E., Ratliff, F., 1980. Bicuculline enhances a negative component and diminishes a positive component of the visual evoked cortical potential in the cat. Proc Natl Acad Sci U S A 77, 7476-7478.

Figure legends

Figure 1. Experimental paradigm. **A** Stimuli types, from the top to the bottom: upper left (UL), down left (DL), upper right (UR), down right (DR) and central. In the actual experimental paradigm the order of the stimuli was randomized. **B** The distribution of the stimulus-onset-asynchronies (SOA) across the subjects.

Figure 2. fMRI regressor construction from single trial ERP differences. Single-trial ERPs were averaged across 5 occipital channels in each hemisphere (1), the amplitude was measured in a pre-defined window(2), the right-hemisphere amplitude was subtracted from the left-hemisphere amplitude to produce a single value for each trial (3), the positive values and the absolute values were separated in two vectors (4) and convolved with canonical HRF (5).

Figure 3. Grand-averaged event-related potentials of 10 subjects recorded inside the MRI scanner. **A.** Central stimulus responses, average across electrodes O1, P7, PO3, P5, PO7 (left panel) and O2, P8, PO4, P6, PO8 (right panel) **B**. The responses to the stimuli in the left (red line) and right (blue line)visual field stimuli averaged across electrodes O1, P7, PO3, P5, PO7 (left panel) and O2, P8, PO4, P6, PO8 (right panel). **C**. The responses to the upper (red line) and lower (blue line) visual fields. Left panel represent the average of contralateral electrodes (O1, P7, PO3, P5, PO7 for right visual field and O2, P8, PO4, P6, PO8 for left visual filed) and the right panel represents the average of ipsilateral electrodes (O2, P8, PO4, P6, PO8 for right visual filed and O1, P7, PO3, P5, PO7 for left visual field)

Figure 4. Scalp voltage distribution and sLORETA source localization for P1 (upper half of the figure) and N1 (lower part of the figure)components for left (left half of the figure) and right (right half of the figure) visual fields. Note different scales for P1 and N1.

Figure 5 fMRI activations to the stimuli in four quadrants and their contrast values with 90% confidence interval bar. $P<0.05$ (FDR) except UL condition with $p<0.056$ (FDR).

Figure 6. fMRI activations to the stimuli in the left and right visual fields and their contrast values with 90% confidence interval bars. $P<0.05$ (FWE).

Figure 7. EEG-predicted fMRI activations for P1 (upper middle panel) and N1 (lower middle panel). The contrast values in 4 ROIs across the subjects are presented to each side of the corresponding fMRI activations. Asterisks mark significant difference with $p<0.05$.

Table 1

Table 1. ERP amplitudes, μV (mean±SE)

Component	Hemisphere	Visual field		
		Left	**Right**	**Central**
P1	**Left**	-0.04±0.35**	0.89±0.40	0.2±0.49
	Right	1.85±0.52	0.2±0.26	1.89±0.71
N1	**Left**	0.92±0.78**	-3.59±0.57***	1.69±0.61
	Right	-3.56±0.51	0.49±	1.15±0.95

Significant differences between right and left hemisphere(t-test with Bonferroni correction):

** $p<0.01$, *** $p<0.001$

Table 2

Table 2. The percentage of correct prediction of the laterality of visual field by single-trial between-hemisphere ERP differences for each subject. Values significantly higher than 50% ($p<0.05$) are given in **bold**

	LVF predicted by P1 in RH	RVF predicted by P1 in LH	LVF predicted-by N1 in RH	RVF predicted-by N1 in LH	P1 in LH predicting RVF	P1 in RH predicting LVF	N1 in RH predicting LVF	N1 in LH predicting RVF	Total P1 predicting visual field	Total N1 predicting visual field
S1	**60**	44	**59**	**61**	52	52	**60**	**60**	52	**60**
S2	**59**	**63**	**69**	**65**	**61**	**62**	**67**	**68**	**61**	**67**
S3	49	46	55	**72**	48	48	**66**	**62**	48	**64**
S4	53	50	**59**	56	51	51	57	58	51	**57**
S5	**64**	52	**79**	**70**	**59**	57	**72**	**77**	**58**	**74**
S6	63	55	**69**	**64**	**60**	**59**	**66**	**67**	**59**	**66**
S7	**59**	57	**60**	**74**	58	58	70	65	**58**	**67**
S8	56	47	52	**64**	52	51	59	57	51	**58**
S9	55	48	54	**58**	52	51	56	56	51	56
S10	47	**59**	**73**	**68**	53	53	70	**72**	53	**70**

LVF –left visual field

RVF – right visual field

LH – left hemisphere

Table 3

Table 3. Event-related fMRI activations (random effect analysis, degrees of freedom=[1,36])

Brain region	Brodmann area	Hemisphere	MNI coordinates			T value	Cluster size
			X	Y	Z		
UL-(UR+DR+DL)**							
Lingual gyrus	18	R	4	-76	-4	5.47	31
Cerebellum	NA	R	18	-70	-8	5.08	11
UR-(UL+DR+DL)*							
Lingual gyrus	18	L	-16	-78	-10	6.57	206
Cuneus		L	-27	-83	24	4.58	7
DL-(UL+UR+DR) *							
Cuneus	18	R	12	-94	6	6.79	66
DR-(UL+UR+DR)*							
Middle occipital gyrus	18	L	-14	-92	12	6.27	2
(UL+DL)-baseline ***							
Inferior temporal gyrus	37	R	45	-70	-2	6.39	192
Medial frontal gyrus	6	L	-8	0	62	5.8	30
Fusiform gyrus	37	R	36	-58	-16	5.68	50
Precentral gyrus	6	R	52	0	38	5.07	3
Cuneus	7	R	22	-81	30	5.28	7
(UR+DR)-baseline ***							
Middle occipital gyrus	19	L	-48	-76	-10	8.98	130
Medial frontal gyrus	6	L	-5	-2	56	7.37	35
Medial frontal gyrus	32	L	-6	8	50	5.93	1
Fusiform gyrus	19	L	-44	-67	-18	6.86	5
Cerebellum	NA	L	-30	-68	-20	6.21	4
Cerebellum	NA	L	-38	-66	-22	6.88	9
Cerebellum	NA	L	-28	-52	-18	8.17	87

Activations above the following threshold:

*- p<0.05 FDR

** p<0.056 FDR

*** p<0. 05 FWE

Table 3

Table 4. P1-amplitude-fMRI correlated areas (fixed-effects analysis, degrees of freedom=[1,5680])

Brain region	Brodmann area	Hemisphere	MNI coordinates			T value	Cluster size
			X	Y	Z		
(P1 larger in the left hemisphere) – baseline ***							
Middle occipital gyrus †	19	L	-52	-78	0	6.13	50
Middle Temporal Gyrus	37	R	44	-64	2	5.56	20
Middle Temporal Gyrus	37	R	54	-66	0	5.39	5
(P1 larger in the right hemisphere) – baseline ***							
Precentral gyrus	4	L	-41	-20	62	8.16	240
Precentral gyrus	6	L	-56	4	40	6.14	10
Superior Frontal Gyrus	8	R	8	52	48	6.13	24
Precentral gyrus	6	L	-42	-8	-52	5.57	16
Medial Frontal Gyrus	6	L	-4	-2	52	5.46	13
Precentral gyrus	6	L	-54	-4	50	5.14	3
Middle Temporal Gyrus†	37	R	42	-66	4	5.13	7

Activations above the following threshold:

*** p<0. 05 FWE

†- cluster used in the ROI analysis

Table 5

Table 5. N1-amplitude-fMRI correlated areas (fixed-effects, analysis degrees of freedom=[1,5680]))

Brain region	Brodmann area	Hemisphere	MNI coordinates			T value	Cluster size
			X	Y	Z		
(N1 larger in the left hemisphere) – baseline ***							
Middle occipital gyrus†	37	L	-46	-74	0	8	132
Medial Frontal Gyrus	6	L	-4	0	56	6.17	65
Postcentral Gyrus	3	L	-56	-16	48	5.46	10
Precentral gyrus	4	L	-34	-24	66	5.38	23
Middle Temporal Gyrus	37	R	44	-66	4	4.84	1
N1 larger in the right hemisphere – baseline ***							
Middle occipital gyrus†	19	R	42	-70	4	5.67	18
Precentral gyrus	4	L	-34	-24	54	5.03	6
Precentral gyrus	4	L	-34	-24	64	4.89	2
Precentral gyrus	4		-36	-24	62	4.88	1

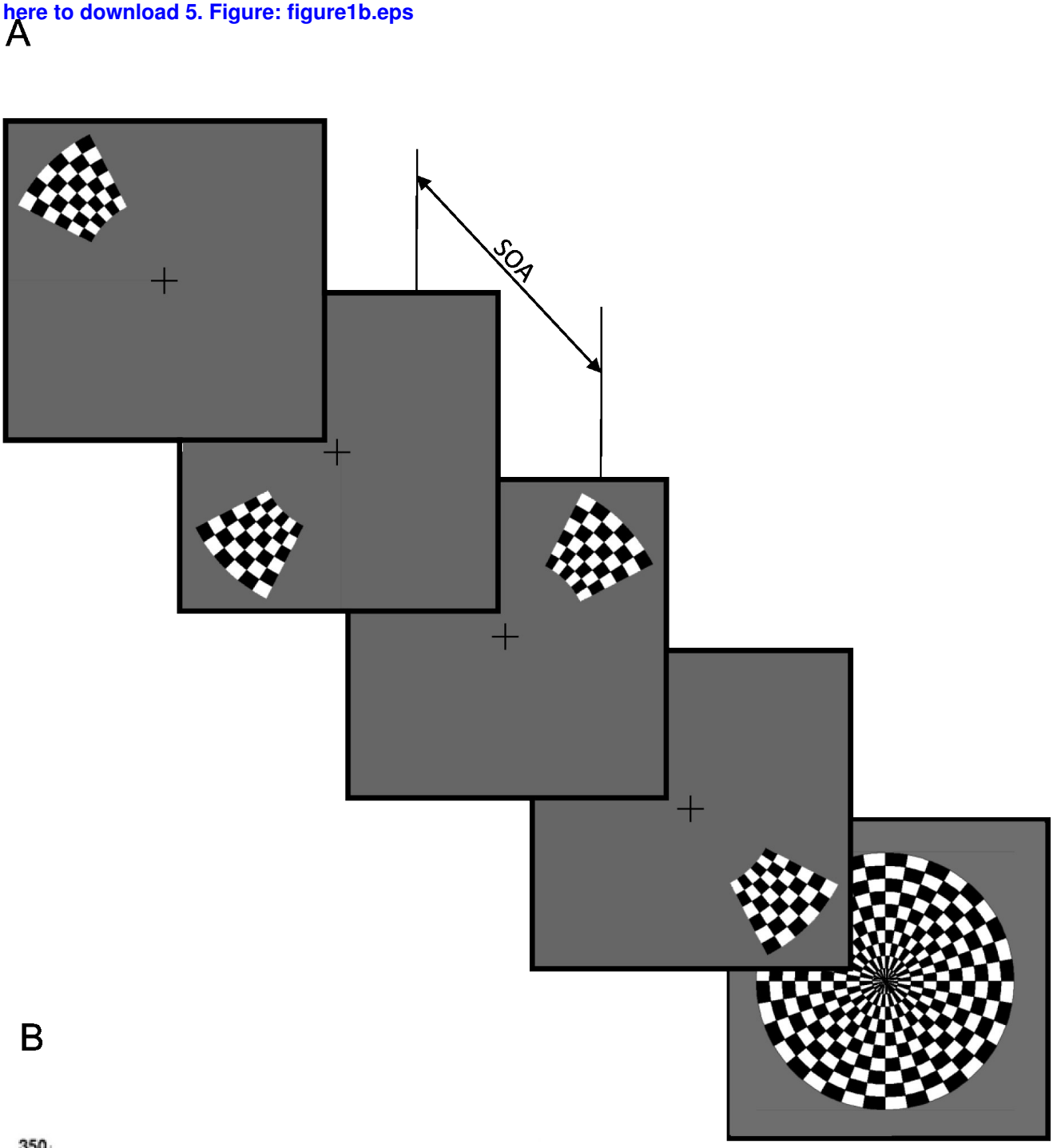
Activations above the following threshold:

*** p<0. 05 FWE

†- cluster used in the ROI analysis

Figure 1

Click here to download 5. Figure: figure1b.eps



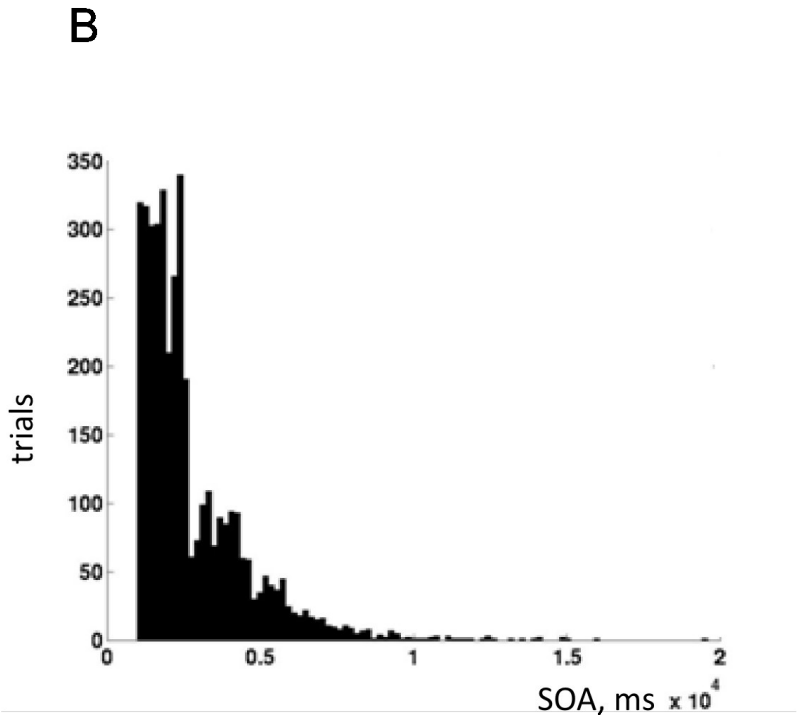


Figure 2

Click here to download 5. Figure: figure2c.eps

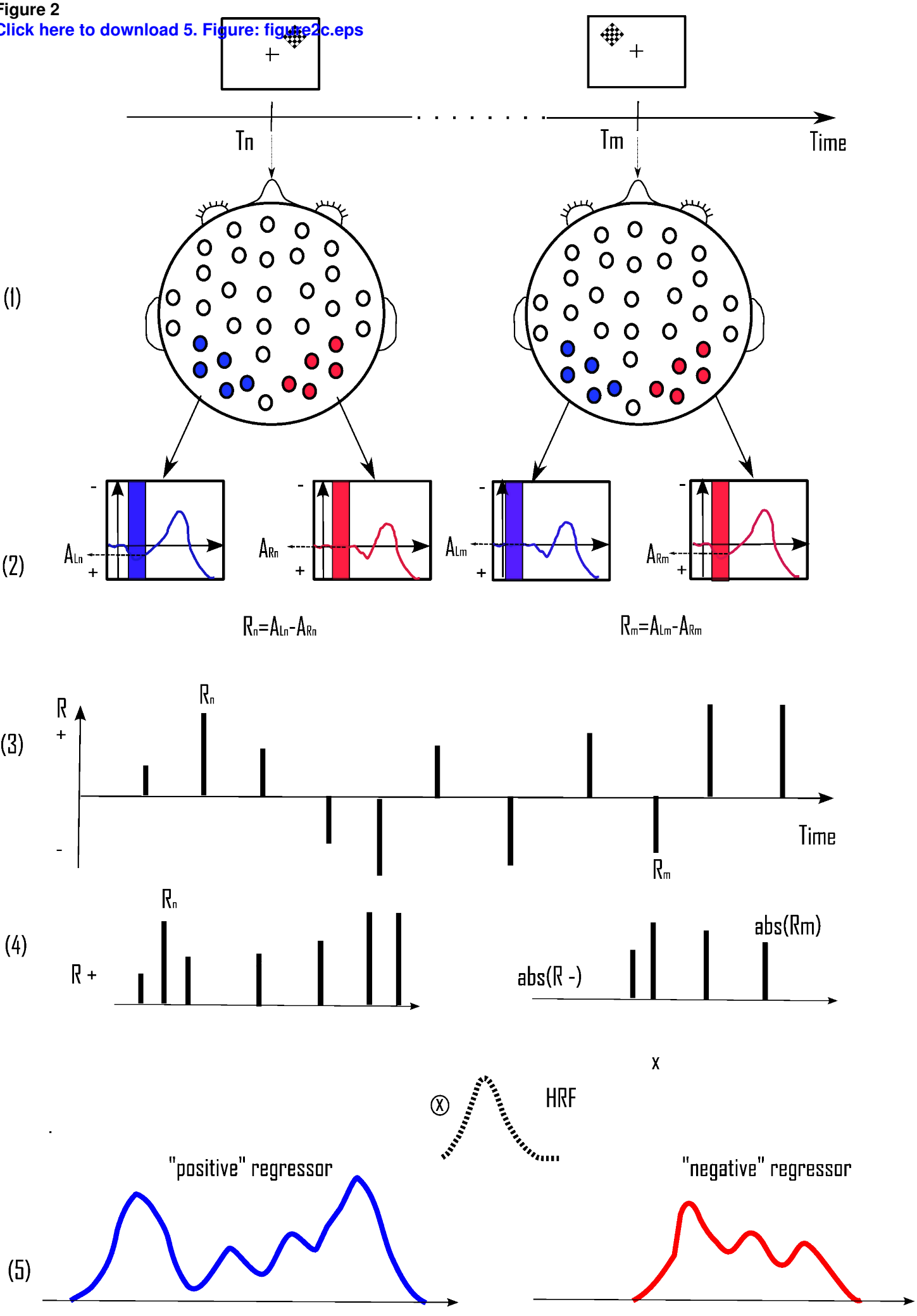


Figure 3

Click here to download 5. Figure: figure3.eps

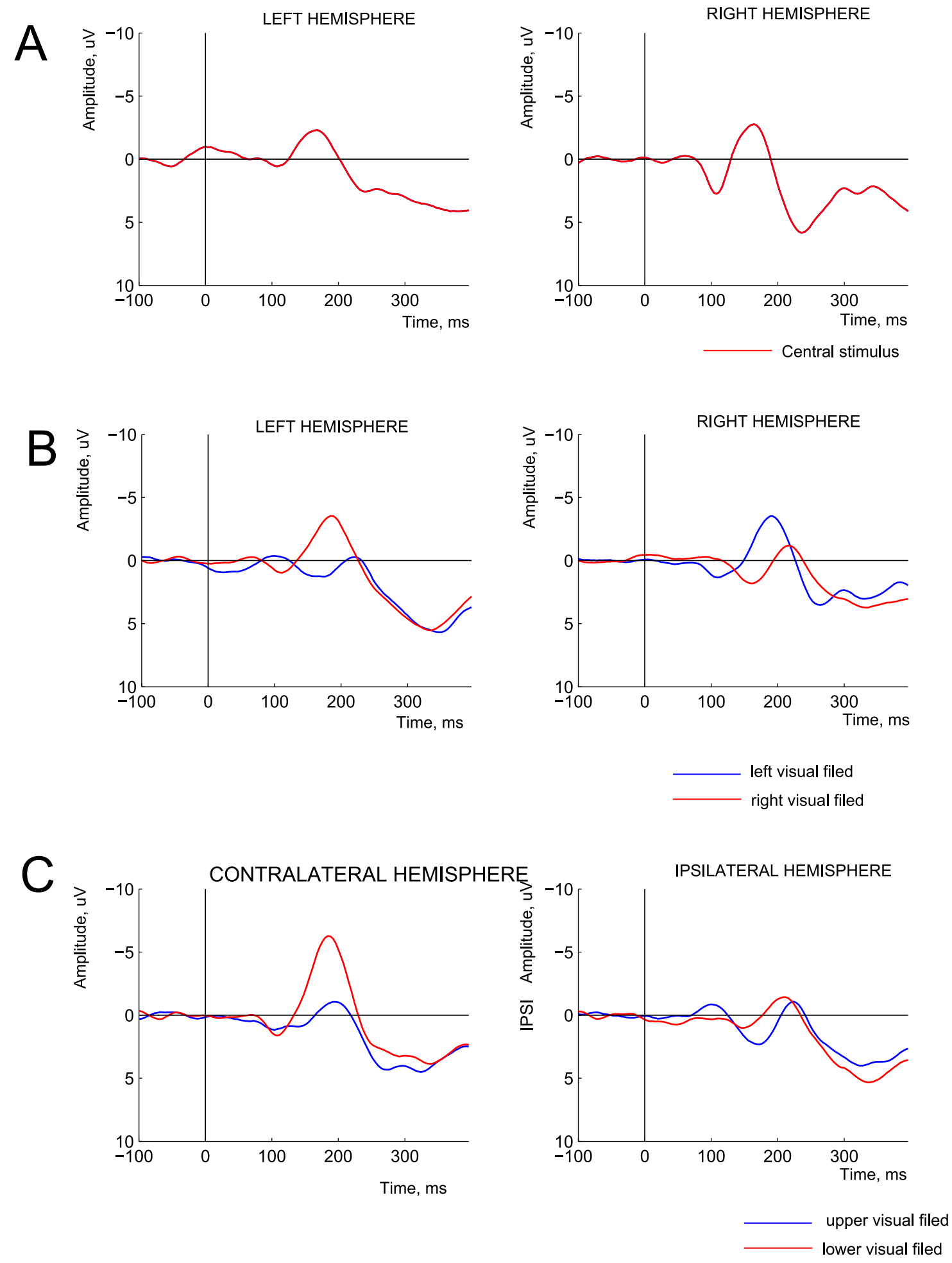
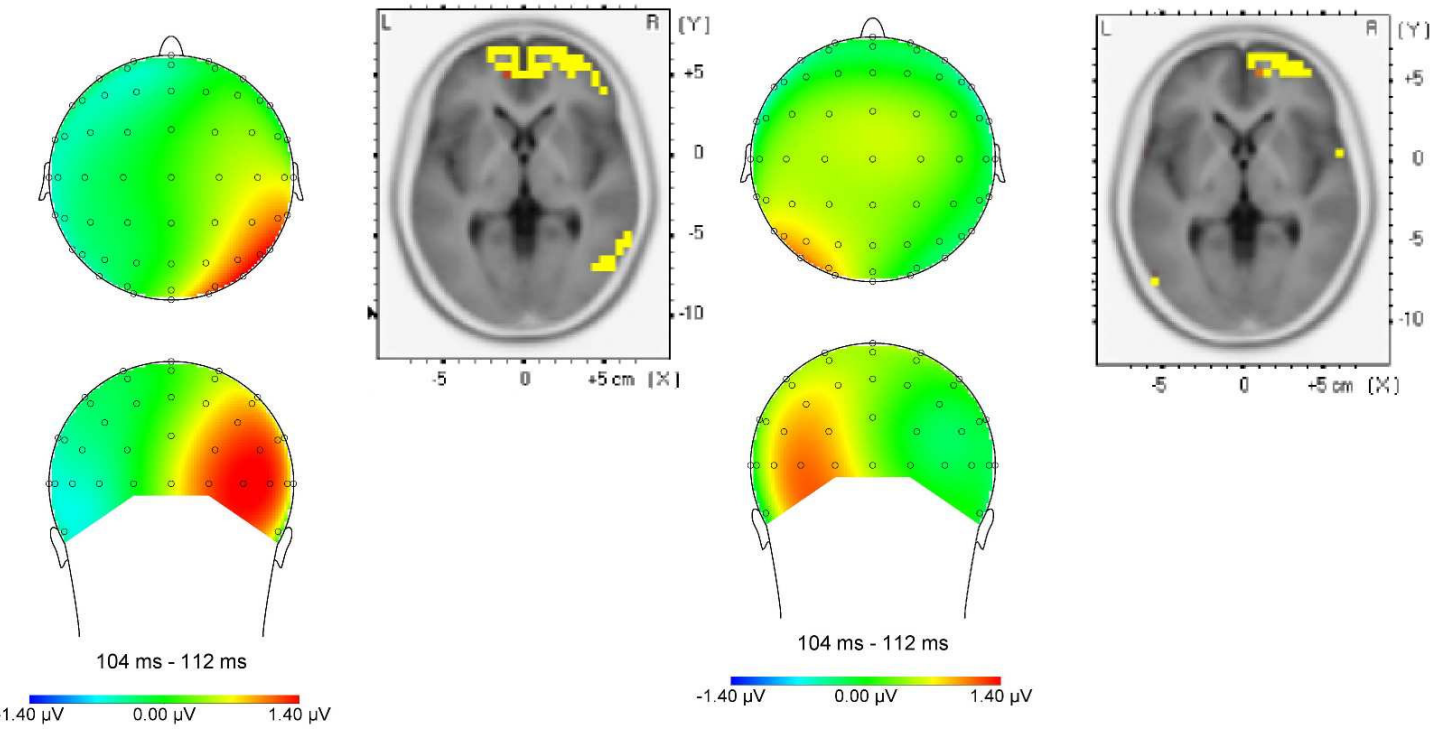
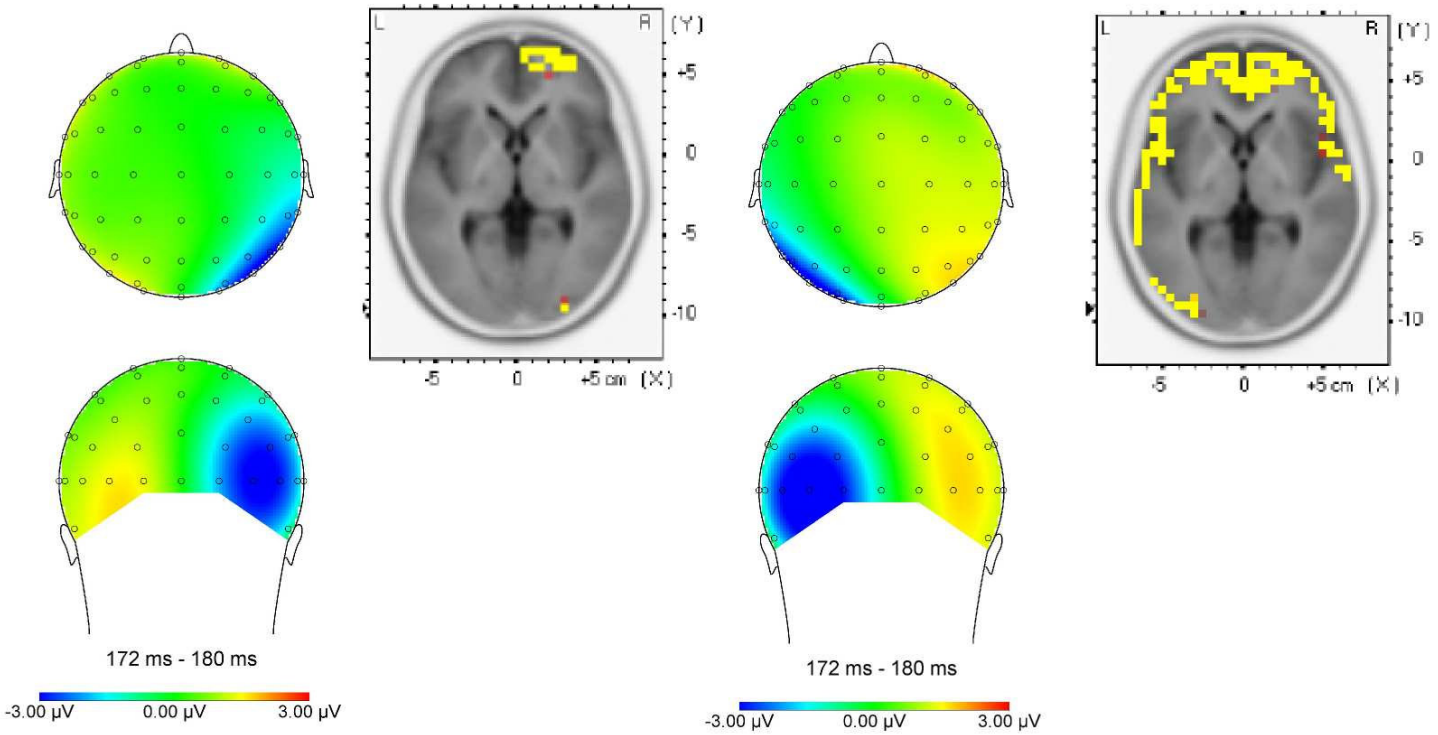


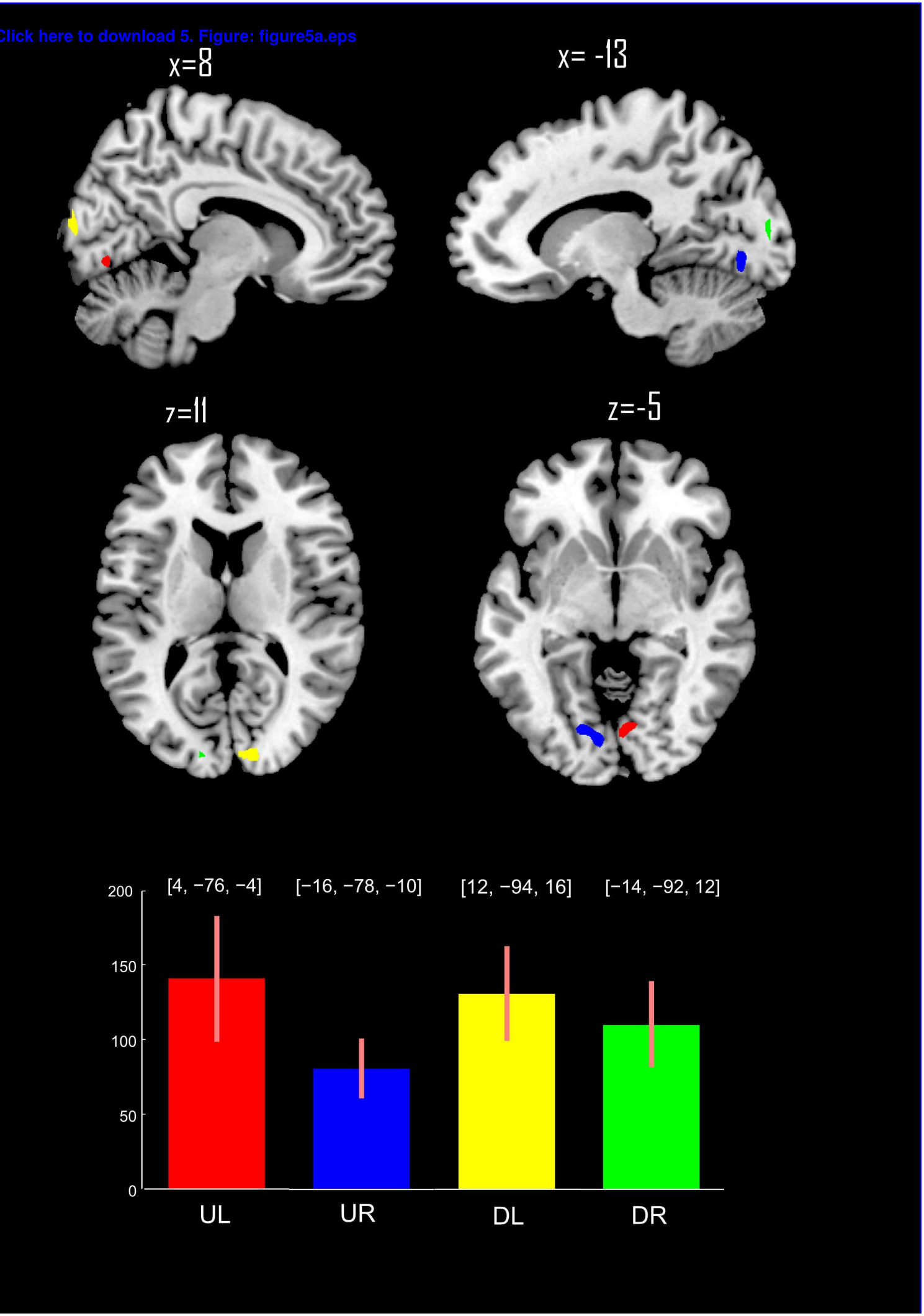
Figure 4

Click here to download 5. Figure: figure4.eps





Click here to download 5. Figure: figure5a.eps



Click here to download 5. Figure: figure6a.eps

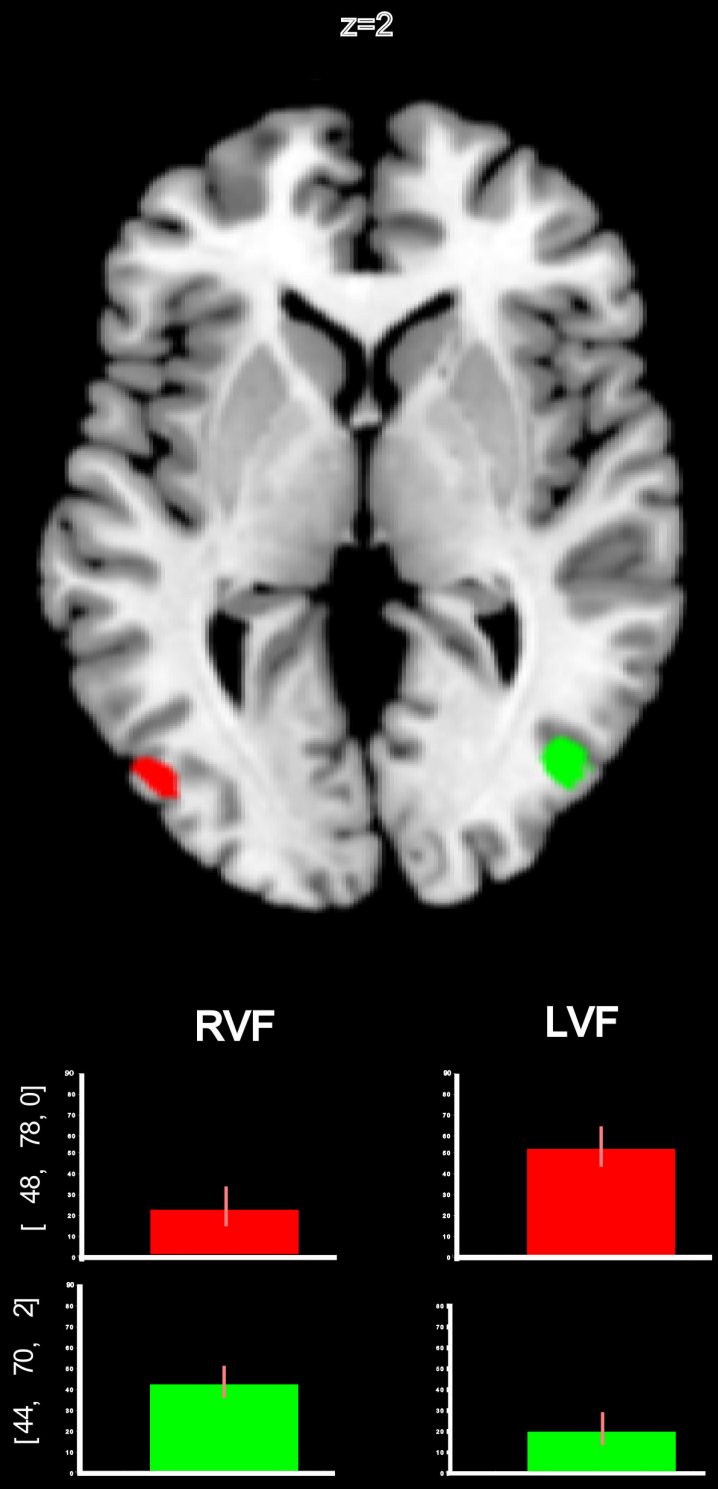


Figure 7
Click here to download 5. Figure: figure7a.eps

